Available online at www.sciencedirect.com

Manufacturing Letters

Manufacturing Letters 35 (2023) 342–349

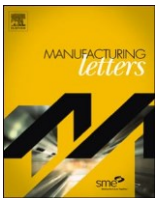

51st SME North American Manufacturing Research Conference (NAMRC 51, 2023)

# Robot forming: automated English wheel as an avenue for flexibility and repeatability

Dean Huang[a,], Derick Suarez[a,], Putong Kang[a], Kornel Ehmann[a], Jian Cao[a,]

[a]*Department of Mechanical Engineering, Northwestern University, 633 Clark St, Evanston 60201, United States*

Abstract

The English wheel is a highly flexible traditional metalworking tool. Currently, English wheeling is a manual manufacturing process that allows skilled craftsmen/smiths to form compound curves. The geometric accuracy and repeatability of the forming pieces are heavily influenced by human factors. Consequently, its applications in modern production industries are limited due to its mechanism. This paper presents the application of a single-robot automation system in the English wheeling process (i.e., robot forming). The automation system reads simulation-based toolpaths or camera-tracked trajectories, autonomously computes the end-effector trajectory and ensures efficient robotic end-effector motion planning by avoiding workspace constraints in operation setup. The automation system hardware (UR5e robotic arm) setup and software program structures developed are demonstrated. Experiments are conducted to compare the automation system performance against human performance when following the same toolpath data. It is found that the automation system is compatible with various types of trajectory data and the system effectively enhances the accuracy and repeatability of toolpath executions.



*Keywords:* English Wheel; Flexible Metal Forming; Automation; Digital Manufacturing

## 1. Introduction

Metal forming remains a dominant area in manufacturing. With the increasing need for custom parts that can be manufactured at scale, the concept of flexibility has been re-evaluated recently: to meet high productivity in achieving high shape complexity through adequate degrees of freedom while maintaining tight tolerances in physical variation [1]. To meet these flexible demands, traditional metal forming processes including the hammer, English wheel, shrinker/stretcher and spinning lathe have begun to be re-examined and adapted to current industry standards [2]. One such of those processes is the English wheel.

The English wheel is a metalworking tool capable of producing sheet metal parts with compound curvature through local stretching. The typical setup of an English wheel is shown in Fig. 1. It is comprised of a flat upper wheel and a domed bottom wheel held together by a frame. While both wheels can roll in place, the vertical height of the upper wheel remains fixed while the vertical height of the bottom wheel can be adjusted through a threaded lead screw to achieve the desired clearance. An operator would hold the sheet at one end or at its sides while the sheet is engaged between the top and bottom wheels at the desired clearance and proceed to drive the sheet in forward/backward/zig-zag patterns. The manual English wheeling process has several advantages: springback is negligible as the operator's hands act as a soft boundary condition, thinning is minimal leading to good structural integrity, and non symmetric shapes can be formed leading to

Equal contribution
Corresponding author
*E-mail address:* jcao@northwestern.edu (Jian Cao).

a wide variety of possible designs although highly non-shallow local features are not feasible. Several challenges arise from the English wheeling process that have deterred it from industry adoption. At its core, traditional English wheeling is an art-form. Smiths spend years learning the craft, able to intuitively know what patterns and pressure to apply while actively receiving tactile feedback from the sheet throughout the driving motion. From a mechanics standpoint, the metal sheet undergoes complex plastic deformation after each pass. Limited Finite Element Method (FEM) studies on a single pass of the English wheel [3] [4] have been performed, and the relationship between the driving path and the final shape is still not well understood, even more so for multiple passes. The first step in industry adoption of the English wheel would be its automation, leading to repeatability, which is the focus of this paper. Robot forming has become more popular with the advent of flexible manufacturing processes such as Double Sided Incremental Forming (DSIF) [5]. Robot forming has also been applied to traditional metal forming processes such as the shrinker/stretcher [6] [7], with recent advances in knowledge based approaches [8]. While automation of the English wheel has been suggested and performed in an architectural context [9], a robust and technical depiction of the repeatability of an automated framework has not.

In this paper, a single-robot automation system for the English wheeling process is developed in which the designed toolpaths are processed and converted to robot end-effector trajectories. The trajectory generation algorithm will first compute the wheeling point motion based on toolpaths coordinate data and transform it to the robot tool center point (TCP) trajectory. The wheeling point is defined as the point at which the wheel is in contact with the sheet. Additionally, a TCP update algorithm is developed and applied to iteratively update the TCP to coincide with the wheeling point at each time step as the robot follows the generated trajectory. The trajectory generation algorithm enables the robot to follow an efficient path in 3-D space that avoids workspace constraints and large joint motions through joint limit implementation. The following sections discuss the physical setup and tool path plan for the proposed experiments, the details of the developed algorithms, and the experimental results that highlight the repeatability of parts made through the automated English wheeling process.

## 2. Methods

### *2.1. Physical setup and experimentation plan*

The setup for the automated English wheeling process is shown in Fig. 2, pertinent dimensions are shown in Fig. 1. An F1.2 710 28-Inch Throat English wheel manufactured by KAKA Industrial is utilized. The top and bottom wheels have a lateral radius of 101.6 mm ($r_{t,l}$) and 38.1 mm ($r_{b,l}$), respectively. The frontal radius of the bottom wheel is 76.2 mm ($r_{b,f}$). Both wheels have a frontal width ($w_f$) of 50.8 mm. An UR5e robotic arm manufactured by Universal Robot is utilized. A polycarbonate L adaptor is designed to connect the robot to the sheet. The center outer edge of the sheet is clamped down to the L adaptor using two C-clamps.

The robotic arm and control commands can be communicated through both offline programming and real-time control communication via RoboDK simulation software.

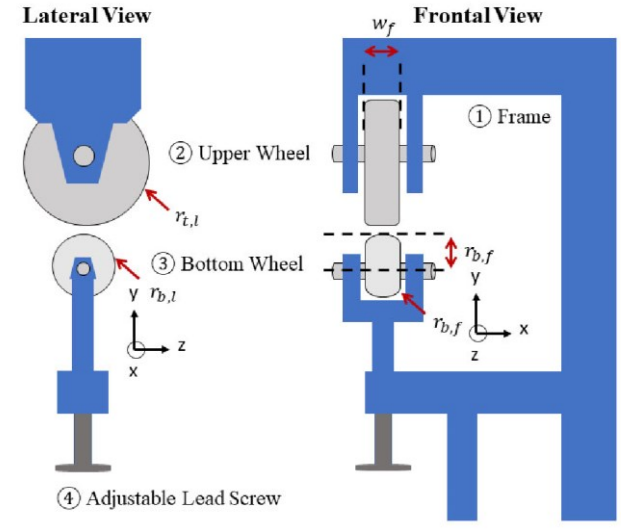


Fig. 1. Key components of the English wheel and wheel dimensions

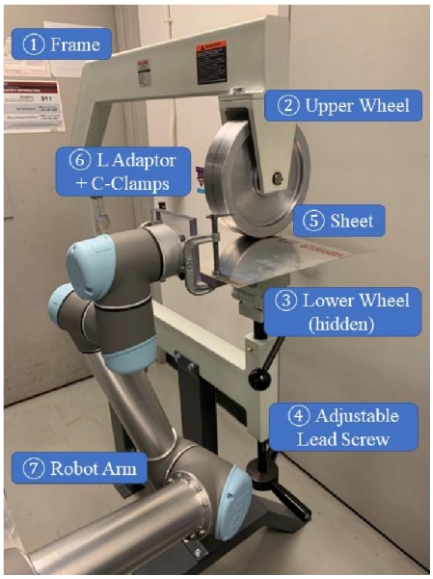


Fig. 2. Robot forming: automated English wheel setup

Offline programming can be achieved by programming script files in the URScript programming language that can be directly uploaded to the UR5e processor and converted into UR5e readable .urp execution files. Real-time robot control communication is achieved by connecting the UR5e robot to the host computer via an Ethernet cable. Once the connection is established, robotic commands in the URScript programming language can be directly sent to the robotic arm for command executions via RoboDK simulation software.

Two trials are performed using 80 320 mm and 260 320 mm sheets of Aluminium alloy 2024-T3 with a thickness of 0.5 mm. The clearance between the top and bottom wheel is kept constant in both trials by keeping the threaded lead screw height at a fixed position after inserting the sheet. Fig. 3 depicts the toolpaths of both trials. Both trials start 120 mm away (z-direction) from the bottom edge to avoid the potential collision between the top wheel and the L adaptor or C-clamps. Trial 1 has a 120 mm straight line (y-direction) tool path. Beginning from the starting point (green), the sheet will be pulled back and then forward returning to the original position as one cycle, for a total of 10 cycles. Three samples of trial 1 are performed through the automated wheeling process and three samples are done manually by hand. Trial 2 follows a zig-zag/triangular pattern. Beginning at the starting point (green), the sheet will be rotated and pulled/pushed to follow the path. Once the end of the path is reached, the path is reversed, returning to the original position to complete one cycle. Three samples of trial 2 are conducted through the automated wheeling process.

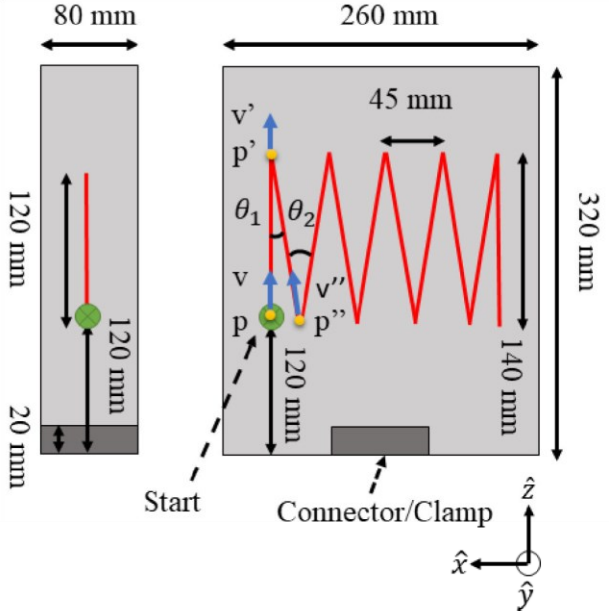


Fig. 3. Trial toolpaths (shown in red) used in trial 1 (left) and trial 2 (right) along with points and vectors discussed in Section 2.2

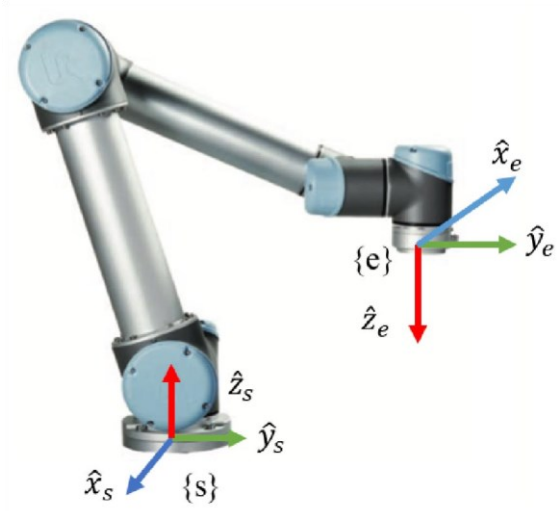


Fig. 4. UR5 base frame fsg and end-effector frame feg demonstration

### 2.2. Wheeling point trajectory generation

The wheeling point is defined as the point where the metal sheet is in contact with the English wheel at every instance. The rotation and translation required to transform the current wheeling point, p 2 $R^3$, to the wheeling point at the next time step, $p^0$ 2 $R^3$, can be described by the transformation matrix $T_{pp0}$ 2 $R^{4\,4}$. Alternatively, the transformation matrix $T_{pp0}$ can also be decomposed into its corresponding Euler angle representation, which specifies the required *ZYX*-axis rotation angle, and Cartesian coordinate translation. Section 2.2 outlines the process to generate wheeling point trajectory in both forms.

Let v 2 $R^3$ and $v^0$ 2 $R^3$ be two normalized vectors that define the direction that p and $p^0$ point to respectively (i.e., the orientation of p and $p^0$ shown in Fig. 3). Note that the initial orientation v at $t = 0$ *s* needs to be specified to perform a series of calculations for all wheeling points.

The rotation axis, ωˆ 2 $R^3$, and the rotation angle, θ, that defines the rotation to align v with $v^0$ is calculated by the following equation:

$$\omega\hat{} = v \quad v^0 \tag{1}$$

$$\theta = cos^{-1}(v \quad v_0) \tag{2}$$

Given the physical setup, the workspace of the robot is constrained by the shape and position of the robot adaptor, English wheel, and metal sheet. Implementing joint limits is an effective way to avoid reaching workspace constraints. The rotation angle θ is restricted to $[-\frac{\pi}{2}, \frac{\pi}{2}]$. The constrained rotation angle $\theta_c$ will be calculated as:

$$\theta_c = \theta\theta \text{ if } -\frac{\pi}{2} \theta \frac{\pi}{2} \tag{3}$$

The rotation matrix, $R_{vv0}$ 2 $R^{3\,3}$, that rotates v around the rotation axis ωˆ by angle $\theta_c$ to align with $v^0$ can be calculated as: $R_{vv0} = (cos\theta_c)I + (sin\theta_c)[\omega\hat{}\,] + (1 + cos\theta_c)(\omega\hat{}\,\omega\hat{}\,)$ (4)

where $[\omega\hat{}\,]$ 2 $R^{3\,3}$ is the cross product matrix of ωˆ , ωˆ ωˆ 2 $R^{3\,3}$ is the outer product and I 2 $R^{3\,3}$ is the identity matrix. The

translation required to move from p to $p^0$ can be simply expressed as $p^0 - p$.

Hence, the transformation matrix $R_{pp0}$ is calculated as:

$$T_{pp0} = \begin{bmatrix} R_{vv0} & p_0 - p \\ 0 & 1 \end{bmatrix} \quad (5)$$

different from the conventionally defined tool-frame transformation, where the tool-frame translation is performed first, followed by the tool-frame rotation. The reversed order of operation (i.e., perform the tool-frame rotation first, followed by the tool-frame translation) ensures that the TCP motion in space aligns with desired orientation first and then translates to the desired location. Additionally, the TCP will be iteratively updated to coincide with the wheeling point at each time step. The TCP update algorithm that performs the update will be introduced in Section 2.4. Fig. 4 and Fig. 5 illustrate all

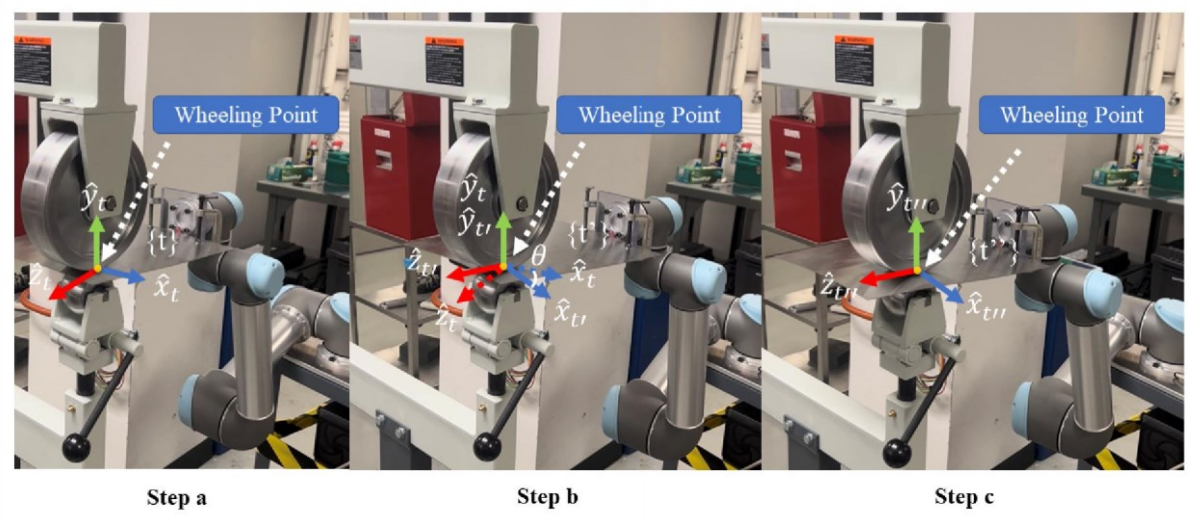


Fig. 5. Illustration of frame transformation from pre-rotational frame ftg (step a) to post-rotational frame ft'g (step b) and to post-translation frame ft"g (step c)

where $p^0$–p is the translation required to move from the current wheeling point p to $p^0$ at the next time step.

Fig. 3 demonstrates the transformation from the starting point *p* to $p^{00}$. The first part of the transformation from *p* to $p^0$ involves translation only, whereas the transformation from $p^0$ to $p^{00}$ involves both rotation ($\theta_1$) and translation.

To decompose the rotation matrix $R_{vv0}$, Slabaugh [10] developed techniques that convert rotation matrices into their corresponding Euler angles. The conversion process will be denoted as $f_\theta(\ )$ in the following sections. The rotations can be expressed in Euler angles as $f_\theta(R_{vv0})$ and the translations can be expressed as $p^0 - p$. Note that the z-axis rotation angle derived from $f_\theta(\ )$ is arbitrary as vectors' co-linearity is independent of the z-axis rotation. Hence, the z-axis rotation should be specified in the tool path design to define the metal sheet inclination angle.

### *2.3. Tool center point (TCP) trajectory generation*

The TCP configuration is defined by the transformation matrix as $T_{st} \in R^{4\times4}$ which describes the configuration of the TCP frame relative to the base frame at the current time step. The TCP will first perform the tool-frame rotation and then the tool-frame translation to reach the desired configuration at the next time step. Note that the motion of the TCP is distinctly

defined frames for trajectory generation where s is the base frame, t is the pre-rotational frame, t' is the post-rotational frame, and t" is the post-translation frame.

The tool-frame rotation from step a to step b shown in Fig. 5 is defined by the following equation:

$$T_{st0} = T_{st}\, Rot_{tt0}(\omega, \hat{\theta}) \quad (6)$$

where $T_{st0} \in R^{4\times4}$ represents the post-rotation tool frame ft'g relative to the base frame fsg, $T_{st}$ represents the pre-rotation tool frame ftg relative to the base frame fsg, which is obtained from the forward kinematics of the robot, $Rot_{tt0}(\omega,\hat{\theta}) \in R^{4\times4}$ is the tool-frame rotation matrix that rotates the pre-rotation tool frame ftg by angle θ about rotation axis $\hat{\omega}$ defined in the pre-rotation tool frame ftg to reach the post-rotation tool frame ft'g. The rotation matrix $Rot_{tt0}(\omega,\hat{\theta})$ is defined as:

$$Rot_{tt0}(\omega,\hat{\theta}) = \begin{bmatrix} R_{tt0} & 0 \\ 0 & 1 \end{bmatrix} \quad (7)$$

where $R_{tt0} \in R^{3\times3}$ is the consecutive ZYX Euler angles rotation required to rotate the pre-rotation tool frame ftg to the post-rotation tool frame ft'g. Note that the wheeling point trajectory (TCP frame trajectory) is the inverse of the tool path. For instance, in order to create a forward path on the metal sheet, the robot end-effector will need to move backward, given that the English wheel is fixed in space. Hence, $R_{tt0}$ is defined as:

$$R_{tt0} = -1\ R_{vv0} \tag{8}$$

where $R_{vv0}$ is the wheeling point rotation matrix at the current time step defined in Section 2.2.

Substituting Eq. (7) into Eq. (6), the post-rotation configuration relative to the base frame fsg is defined by:

$$T_{st0} = \begin{bmatrix} R_{st}R_{tt^0} & P_{st} \\ 0 & 1 \end{bmatrix} \tag{9}$$

where rotation matrix $R_{st} \in R^{3\times3}$ and translation vector $P_{st} \in R^3$ represents the rotation and translation of the transformation matrix $T_{st}$ (i.e., the configuration of the pre-rotation tool frame ftg relative to the base frame fsg)

The tool-frame translation from step b (i.e., the post-rotation configuration $T_{st0}$) to step c (i.e., the desired post-translation configuration) at the next time step is defined by the following equation:

$$T_{st00} = T_{st0}\ \ Trans_{t0t00}(P) \tag{10}$$

where $T_{st00} \in R^{4\times4}$ represents the post-translation tool frame ft"g relative to the base frame fsg, $Trans_{t0t00}(P) \in R^{4\times4}$ is the translation matrix that translates the post-rotation frame ft'g by P defined in post-rotation tool frame ft'g to reach the post-translation tool frame ft"g. The translation matrix $Trans_{t0t00}(P)$ can be defined as:

$$Trans_{t0t00}(P) = \begin{bmatrix} I & P_{t0t00} \\ 0 & 1 \end{bmatrix} \tag{11}$$

where $I \in R^{3\times3}$ is identity matrix and $P_{t0t00} \in R^3$ is the translation required to translate from the post-rotation frame ft'g to the post-translation tool frame ft"g.

Similar to the derivation of the rotation matrix, $R_{tt0}$, since the wheeling point trajectory is the inverse of the tool path, $P_{tt00} \in R^3$ is defined as:

$$P_{tt00} = \ \ 1\ (p^0 \ \ \ p) \tag{12}$$

where $P_{tt00}$ represents the translation required to translate from the pre-rotation tool frame ftg to the desired post-translation tool frame $ft^{00}g$. To derive $P_{t0t00}$, the frame rotation due to the rotation matrix $Rot_{tt0}(\omega,\hat{\theta})$ needs to be considered. Hence, the translation vector, $P_{tt00}$, defined in the pre-rotation tool frame ftg needs to be defined in the post-rotation tool frame $ft^0g$. The change of reference frame is implemented through the static frame transformation, which defines $P_{t0t00}$ as:

$$\begin{aligned} P_{t0t00} &= T_{tt0}\begin{bmatrix} 1 \\ P_{tt^{00}} \end{bmatrix}^T \\ &= Rot_{tt0}{}^{1}(\omega,\hat{\theta}\ \ )\ {}^{h}P_{tt00}{}^{T}\,1^{i^T} \end{aligned} \tag{13}$$

where $T_{tt0}{}^{1} \in R^{4\times4}$ is the inverse of the transformation matrix $T_{tt0}$. Since $T_{tt0}{}^{1}$ represents the configuration of the pre-rotation tool frame ftg relative to the post-rotation tool frame ft'g, it is equivalent to $Rot_{tt0}{}^{1}(\omega,\hat{\theta}) \in R^{4\times4}$. ${}^{h}P_{tt00}{}^{T}\,1^{i^T} \in R^4$ is the translation vector $P_{tt00}$ written in homogeneous coordinates for dimensional consistency.

Substituting Eq. (9), Eq. (11) and Eq. (13) into Eq. (10), the post-translation configuration relative to the base frame fsg is defined as:

$$T_{st} = \begin{bmatrix} R_{o\,1o}(\omega,\hat{\theta}) & hP_{tt00}{}^{T}1i^T \\ 0 & R_{tt}\ P_{st} + Rot_{tt}\ 1 \end{bmatrix} \tag{14}$$

### 2.4. TCP Update Algorithm

Since the wheeling point serves as the reference point for trajectory generation at every time step, a TCP update algorithm resets the TCP, which initially locates at the end-effector frame feg (shown in Fig. 4), to the wheeling point frame ftg. As stated in Section 2.3, the transformation from one TCP configuration to the next TCP configuration requires two time steps. Let $k$ be the total number of TCP configurations, then the total number of time steps involved in the TCP trajectory is $2k$. At the initial time step, the configuration of the tool center point (TCP) is set to coincide

with the initial wheeling point configuration, denoted as $T_0 \in R^{4\times4}$. As TCP goes through the cumulative updating process, the TCP configuration at time step $i$, $\forall i \in N$ such that $0 < i \le k$ is:

$$T_i = \begin{cases} T_{i-1}T_{ipp1o}\ldots T_{2pp0}T_{1pp0}T_0 & \text{if } i = 2n, n \in N \\ T_{i-1}Rot_{ipp0}T_{ipp1o}\ldots T_{2pp0}T_{1pp0}T_0 & \text{if } i = 2n+1, n \in N \end{cases} \quad (15)$$

where $T^i_{pp0} \in R^{4\times4}$ is the transformation matrix $T_{pp0}$ derived in Section 2.2 at time step $i$, $Rot^i_{pp0} \in R^{4\times4}$ is the rotation component of the transformation matrix $T_{pp0}$ at time step $i$, defined as:

$$Rot_{pp} = \begin{bmatrix} R^i_{vv0} & 0 \\ 0 & 1 \end{bmatrix} \quad (16)$$

where $R^i_{vv0} \in R^{3\times3}$ is the rotation matrix $R_{vv0}$ derived in Section 2.2 at time step $i$.

## 3. Results

All samples (after wheeling) were scanned with a 7525 ROMER Absolute Arm scanner, volumetric accuracy of 0.029 mm. Fig. 6 and Fig. 7 depict the y-contour (out of plane direction) plots for the wheeled samples for trial 1 and 2,

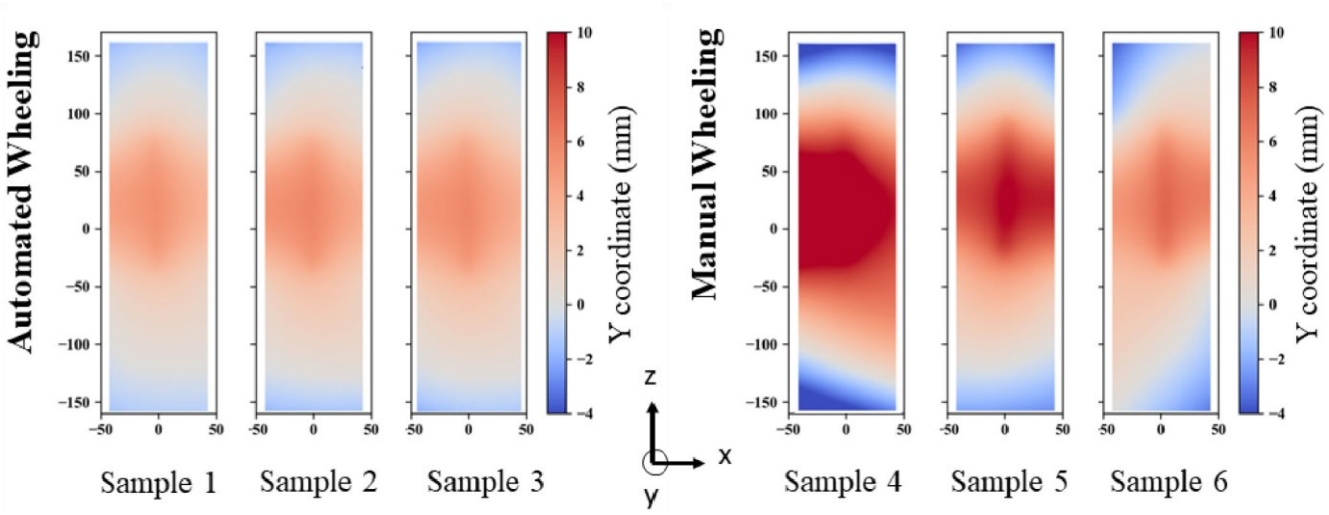


Fig. 6. Trial 1 results (mm): z coordinate plots of formed parts through robot forming (left) and manual forming (right). The deformation pattern for the automated wheeling parts is consistent while the manual one is sporadic.

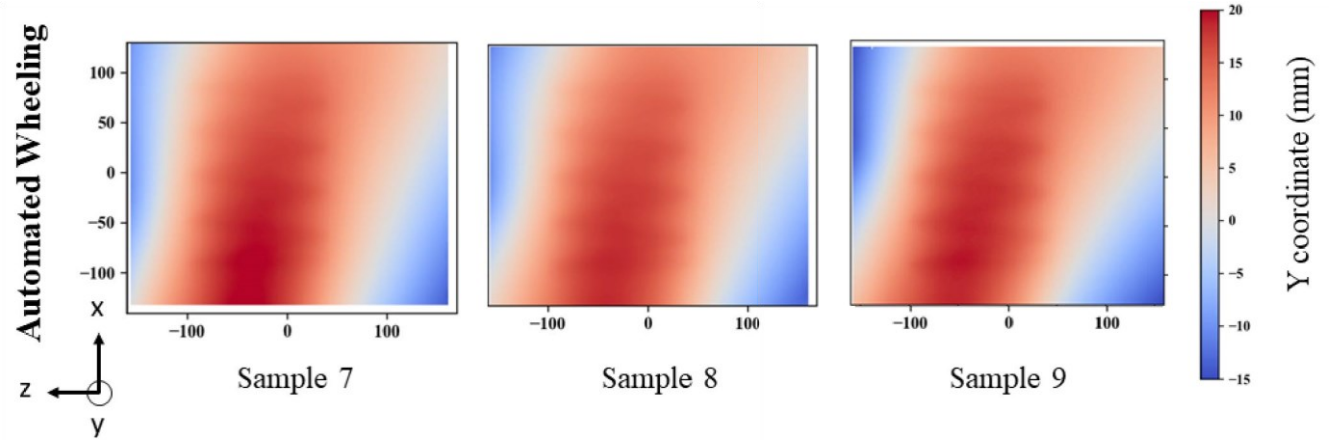


Fig. 7. Trial 2 results (mm): z coordinate plots of formed parts through robot forming. The deformation pattern is consistent.

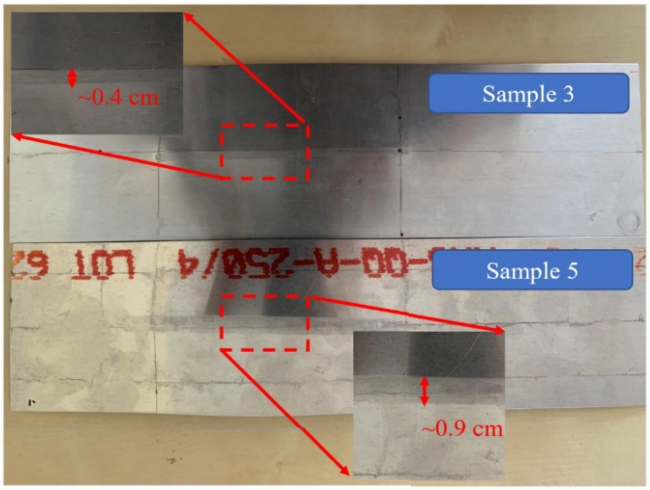


Fig. 8. Robot/manual toolpath width comparison

initially fully aligned. Looking at the L2 distortion values (2.57, 2.90 and 2.87 mm), affirms the repeatability of the automated samples.

Meanwhile, the manual samples have a larger spread of L2 distortion (5.14, 7.14, 3.43 mm). Of note, the curvature of the manual samples is consistently larger than that of the automated wheeling samples. Fig. 8 shows a picture of the top surface of an automated and manual sample from trial 1. The contact mark width for the manual sample (0.9 cm) is much larger than that for the automated sample (0.4 cm). This larger contact area increases the region of local stretching accounting for the larger curvatures in the manual samples. The manual process is less reliable as one can deviate even for a simple tool path of forward and backward strokes, inadvertently increasing the contact area between the sheet and wheels. Moreover, for a manual process, the degree of keeping the sheet gripping fixed (with hands) depends largely on the skill of the operator.

Table 2 lists associated values with the y-contours of Fig. 7. Looking at Fig. 7, even for this more complex toolpath good repeatability is seen, affirmed by the L2 distortion values (11.09, 10.49, 11.13 mm). Note that for this trial, the most important measurement of performance is the consistency of the obtained curvature. Here, the maximum difference between the three samples is 0.64 mm, although larger than that in the automated/robot forming of the straight toolpath case (0.4 mm), it is still smaller than the manual case (0.9 mm) in Trial 1, which is a much simpler toolpath. The y profile is not symmetric, as expected, since although the toolpath is symmetric, the initial deformation occurs at one edge of the sheet and progresses to the other. It was noticed that significant curvature was developed before finishing the first sweep of the zig-zag pattern. The authors hypothesize that this large initial curvature on the side of the sheet where the tool path starts also contributes to the skewness of the final shape. It is suggested to wheel thicker sheets in the future to minimize this effect.

respectively. Table 1 lists associated values with the y contours of Fig. 6: lowest y point, highest y point, and L2 distortion, a measure of how curved/distorted the sample is. For parts with multiple curvatures finding a reference plane can become arbitrary. The distortion measure used here samples the edge points of the scanned part data, finds the best-fit plane from those edge points, then rotates all the points in the scan data as to align the original reference plane with the new best-fit plane. Then the L2 norm of the y distance of all surface points to the plane is taken. This measure was found to work well as an aggregate when comparing the deformation of the sheet and the repeatability of the parts. Other methods to measure local curvature can also be used such as Gaussian curvatures. Looking at the y contour plots of Fig. 6, the automated wheeling samples show repeatability with the overall shapes being consistent and the bulk of the deformation occurring around the tooling path. The contour of the automated wheeling samples leans slightly left (-x direction). With the current setup, the initial contact position between the sheet and wheel is set manually, leading to potential initial misalignment. In the future, a detector will be implemented to ensure the sheet is

It was noticed that the samples made through automated wheeling achieve their final configuration once the grip has been removed. Introducing the fixed grip condition adds a springback effect. While robotic forming improved the repeatability of the process several additional improvements are to be made to achieve less deviation between samples: (1) tight tolerances on the initial curvature of work pieces and their material homogeneity must be enforced, and (2) methods to reduce vibrations in the frame and robot arm. Moreover, using thicker or stiffer sheets will avoid possible elastic buckling of the sheet during the driving motion of the robot. While the toolpaths in the trials shown were in plane with the sheet (the robot arm end effector does not change y position), a 3D movement can be easily implemented given the methodology presented (a 3D or non-linear sequence of points can be specified and the algorithm will work accordingly). Future work will take into account the progressive deformation of the sheet, adjusting the toolpath in 3D. For the trials shown the toolpath was executed successfully. For very high clamping forces between the wheels and sheets, the contact area can present problems for the robot arm when rotating along an arbitrary point - this must also be investigated.

Table 1. Trial 1 sample results (mm): L2 distortion values are more spread out for manual samples than those from robot forming highlighting the repeatability of automated wheeling.

| Sample | Forming | $y_{low}$ | $y_{high}$ | L2 distortion |
|---|---|---|---|---|
| Sample 1 | Robot | -1.69 | 5.47 | 2.57 |
| Sample 2 | Robot | -2.01 | 5.85 | 2.90 |
| Sample 3 | Robot | -2.13 | 5.81 | 2.87 |
| Sample 4 | Manual | -6.50 | 13.67 | 7.34 |
| Sample 5 | Manual | -3.70 | 10.70 | 5.14 |

| | | | | |
|---|---|---|---|---|
| Sample 6 | Manual | -3.69 | 7.21 | 3.43 |

Table 2. Trial 2 sample results (mm): L2 distortion values are fairly consistent showing the repeatability of automated wheeling.

| Sample | Forming | $y_{low}$ | $y_{high}$ | L2 distortion |
|---|---|---|---|---|
| Sample 7 | Robot | -14.05 | 20.56 | 11.09 |
| Sample 8 | Robot | -13.45 | 18.76 | 10.49 |
| Sample 9 | Robot | -15.07 | 19.44 | 11.13 |

## 4. Conclusion

The process of automating the English wheel via a robotic arm was outlined including the algorithms used to determine the robot arm kinematics based on a prescribed toolpath. Results from two separate trials (straight and zig-zag patterns) showed good repeatability of the automated wheel with L2 distortion values for the straight toolpath (2.57, 2.90, 2.87 mm) and zig-zag toolpath (11.09, 10.49, 11.13 mm) closely matching between samples. For the straight tool path, a set of manual experiments was also performed and showed much less repeatability with spread out L2 distortion values of (7.34, 5.14, 3.43 mm).

Several improvements are to be made in future work. In the manual English wheeling process, after a pass, the sheet has become deformed, and as such the smith adjusts the next pass taking into account this deformation. To account for each pass deformation, a feedback system must be implemented to scan the current state of the sheet as to inform the next pass. A combination of compliant grippers and updating the end effector position to account for the current curvature of the sheet are possible methods to more closely mimic manual wheeling. Currently, the clearance of the top and bottom wheel is prescribed through the adjustable lead screw. A small deviation in this clearance can potentially lead to a drastically different clamping force between the sheet and wheels. A method to actively measure this clamping force must be implemented. Additionally, a motor can be added to the bottom lead screw mechanism for more control over the vertical position of the bottom wheel. Moreover, deflection in the frame was noticed as the sheet was more tightly clamped between the wheels. This deflection must be tracked to determine an accurate clearance gap between the wheels while the sheet is inside. Once the automated wheeling process more closely mimics the degree of flexibility of the smiths in a controlled fashion one can start tackling the inverse problem: determining what tool path and with what wheel gap will yield a desired deformed geometry considering springback effects.

## Acknowledgements

The authors would like to acknowledge support from the NSF Engineering Research Center for Hybrid Autonomous Manufacturing Moving from Evolution to Revolution (ERC-HAMMER) under Award Number EEC-2133630.

## References

[1] Yang DY, Bambach M, Cao J, Duflou JR, Groche P, Kuboki T, et al. Flexibility in metal forming. CIRP Annals 2018;67:743–65. doi:10.1016/j.cirp.2018.05.004.

[2] Bowen DT, Russo IM, Cleaver CJ, Allwood JM, Loukaides EG. From art to part: Learning from the traditional smith in developing flexible sheet metal forming processes. Journal of Materials Processing Technology 2022;299:117337. doi:10.1016/j.jmatprotec.2021.117337.

[3] Fann KJ. Finite element study on forming metal sheets with an English wheel. IOP Conference Series: Materials Science and Engineering 2022;1222:012006. doi:10.1088/1757-899x/1222/1/012006.

[4] Bowen DT, Music O, Alaz Erdinc A, Shokrani A, Loukaides EG. Numerical modelling and deformation mechanics of the English wheel process. Forming the Future 2021:457–66. doi:10.1007/978-3-030-75381-8 38.

[5] Peng W, Ou H, Becker A. Double-sided incremental forming: A Review. Journal of Manufacturing Science and Engineering 2019;141. doi:10.1115/1.4043173.

[6] Scherer D, Yang Z, Hoffmann H. Driving – a flexible manufacturing method for individualized sheet metal products. International Journal of Material Forming 2010;3:955–8. doi:10.1007/s12289-010-0927-5.

[7] Opritescu D, Sachnik P, Yang Z, Golle R, Volk W, Hoffmann H, et al. Automated driving by standardizing and scaling the manufacturing strategy. Procedia CIRP 2012;3:138–43. doi:10.1016/j.procir.2012.07.025.

[8] Hartmann C, Opritescu D, Volk W, Schmiedl F, Ritter M, Gritzmann P. A knowledge-based automated driving approach for flexible production of individualized sheet metal parts. Knowledge-Based Systems 2022;244:108558. doi:10.1016/j.knosys.2022.108558.

[9] Rossi G, Nicholas P. Modelling a complex fabrication system - new design tools for doubly curved metal surfaces fabricated using the English wheel. ECAADe Proceedings 2018. doi:10.52842/conf.ecaade.2018.1.811.

[10] Slabaugh GG. Computing euler angles from a rotation matrix. http://eecs.qmul.ac.uk/ gslabaugh/publications/euler.pdf (accessed November 1, 2022).